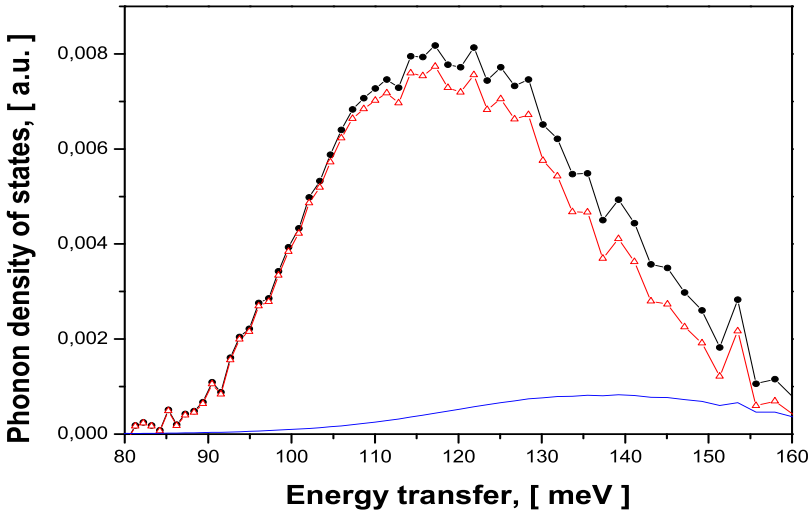

Figure 5.21: Optic modes in phonon density of states for hydrogenated austenitic stainless steel Fe-25Ni-20Cr(at 2.3 GPa) with H/Me=0.30(2), (-●-) experimental data, (—) multiphonon contribution and (-△-) DOS after multiphonon correction.

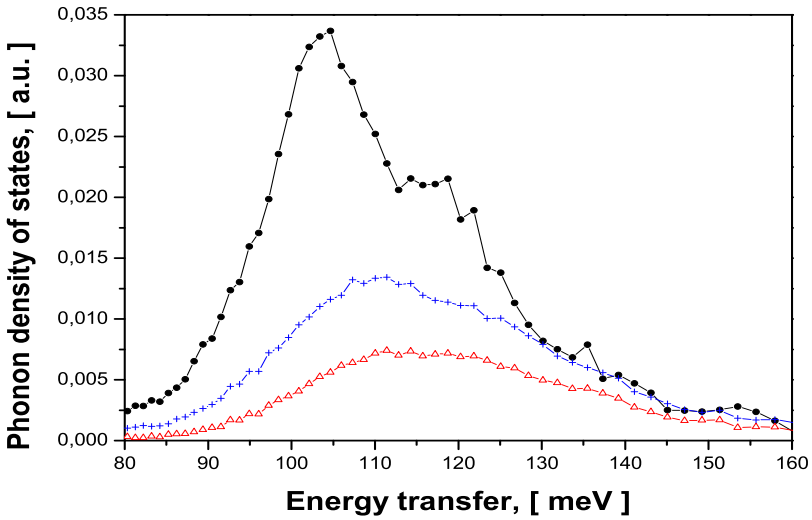

Figure 5.22: Optic modes in phonon density of states for hydrogenated samples of austenitic stainless steel Fe-18Ni-10Cr, (-●-) experimental data for H/Me=1.03(9) at 7.0 GPa, (-+-) experimental data for H/Me=0.56(2) at 3.0 GPa and (-△-) experimental data for H/Me=0.30(2) at 2.3 GPa DOS after multiphonon correction and renormalisation.

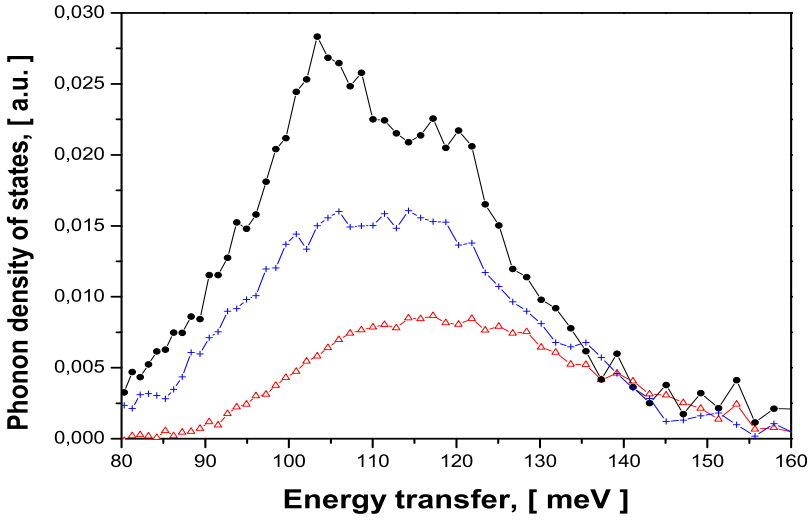

Figure 5.23: Optic modes in phonon density of states for hydrogenated samples of austenitic stainless steel Fe-25Ni-20Cr, (-●-) experimental data for H/Me=0.94(5) at 7.0 GPa, (-+-) experimental data for H/Me=0.66(3) at 3.0 GPa and (-△-) experimental data for H/Me=0.35(2) at 2.3 GPa DOS after multiphonon correction and renormalisation.

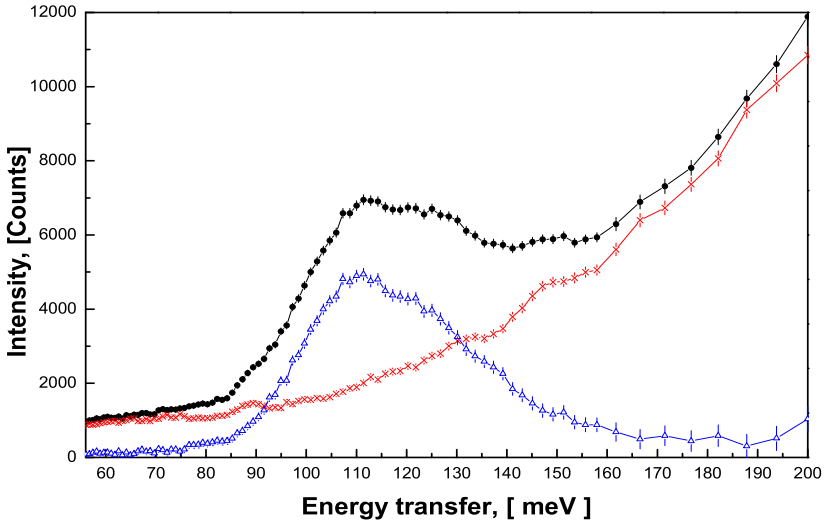

Figure 5.24: Experimental data for phonon DOS in hydrogenated samples of Fe-18Ni-10Cr(H/Me=0.56(2)), (-●-) experimental data for H/Me=0.56(2), (-△-) experimental data for non-loaded Fe-18Ni-10Cr and (-×-) difference.

Contribution of background is strongly dependent on energy(fig. 5.24), because in the high energy region (100 meV) high flux of neutrons exist which passes the neutrons shield. Because of this background grows extremely fast(similar to power law) with energy and this background contribution is much higher than the contribution from the sample. This is the reason why the intensity in the phonon density of states is high even after multiphonon corrections.

5.3 Models and results

5.3.1 Modelling of high hydrogenated samples

On the experimental data for full hydrogenated samples was applied generalised force Born-von Karman model. Fully hydrogenated austenitic stainless steels have rock-salt structure.

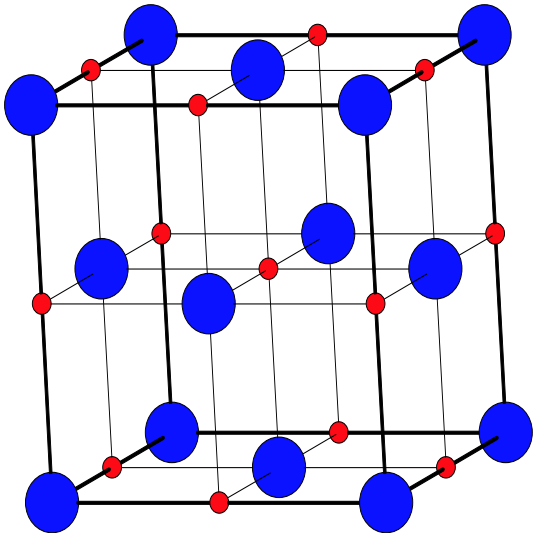

Figure 5.25: Structure model of hydrogenated austenitic stainless steels, (•) metal atoms and (•) hydrogen atoms.

As input parameters force constants between first neighbours were used: metal-hydrogen(2), metal-metal(3) and hydrogen-hydrogen(3). Dynamical matrices for the metal-metal and hydrogen-hydrogen interactions have the same form:

$$\begin{pmatrix} \alpha_1 & \beta_1 & 0 \\ \beta_1 & \alpha_1 & 0 \\ 0 & 0 & \alpha_2 \end{pmatrix}, \tag{5.2}$$

and for metal-hydrogen interaction:

$$\begin{pmatrix} \alpha_1 & 0 & 0 \\ 0 & \alpha_2 & 0 \\ 0 & 0 & \alpha_2 \end{pmatrix}. \tag{5.3}$$

In this model the influence of hydrogen-hydrogen bonding on lattice dynamics was taken into account.

Influence of hydrogen on metal-metal interactions

For the metal-metal force constants in both systems (Fe-18Cr-10Ni and Fe-25Cr-20Ni) values obtained from phonon dispersion curves on the Fe-18Cr-12Ni-2Mo(this study) (table 4.1) without hydrogen were used. These values were corrected by Grüneisen parameter γ. In this modelling approximation was made that lattice expansion due to hydrogenation is equivalent to the thermal expansion. This approximation is valid when electronic properties of the system are not significantly changed. From these values conclusion about behaviour of fully hydrogenated system could be made. It is correct when only lattice expansion and no phase transition occur. This assumption is valid for the austenitic stainless steel Fe-25Cr-20Ni(table 5.1) but not for the Fe-18Cr-10Ni(table 5.1.2). In which is structure change due to phase transition from fcc to hcp. In the case of Fe-18Cr-10Ni the local surroundings for hydrogen is not significantly changed, in this case hydrogen atoms are located in octahedral voids. Influence on acoustic mode is described with the relation:

$$\frac{\Delta\omega}{\omega} = -3\gamma\frac{\Delta a}{a}, \tag{5.4}$$

where a and Δa are lattice parameter and its dilatation respectively. They are obtained from diffraction studies. In the most metallic system a value of Grüneisen parameter γ is around 2.
Firstly simulation of density of states based on the Born-von Karman model with approximation that all metal atoms are identical was used. For the description of the metal-hydrogen interaction only one free parameter(α_1) is applied. Position of the optic modes are determined by (α_1+2α_2). This parameter is determined with energy of hydrogen modes. In the rock-salt structure two conditions for sharp optic peak exist: $m_H \ll m_{Me}$ and weak interaction between light elements. Under these conditions the frequency of hydrogen atom is equal to:

$$\omega = \sqrt{\frac{2A}{m_H}} \tag{5.5}$$

and those width of hydrogen modes in DOS is estimated to:

$$\frac{\Delta\omega}{\omega} = \frac{m_H}{2m_{Me}}. \tag{5.6}$$

The result of these simulations show that dispersion of our system is about 1 meV which confirm relation(eq. 5.6) but it is much less then for dispersion based on experimental data which is about 20 meV. After including the resolution function optic peak became broader(2-5 meV) but still much less than experimental data. Similar relative broadness of the optic mode is observed on other fcc systems with great difference in masses of light and heavy atoms like in US, UN and UC [Weber 1973, Jackman 1986]. In these systems light atoms are located in octahedral voids of the heavy one, which form fcc lattice. For these

systems also exist experimental data for phonon dispersion curves and they confirmed that dispersion of optics modes is very low. It is due to strong Me-H interaction and very weak interaction between light atoms. On the other hand in Pd-D system in which exist very strong D-D interactions with weak metal-hydrogen ones which lead to much broader optic peaks. For $PdD_{0.63}$ a low value of optic branches is characteristic. So the metal-metal interaction is significantly lowered by the influence of deuterium [Rafizadeh 1981].

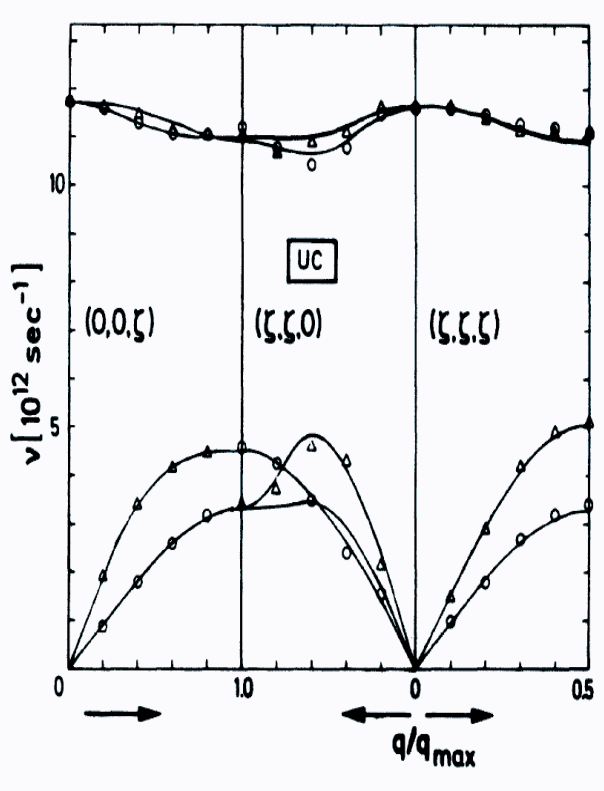

Figure 5.26: Phonon dispersion curves in UC, △ and ∘ show experimental points and (—) represent model calculation [Weber 1973].

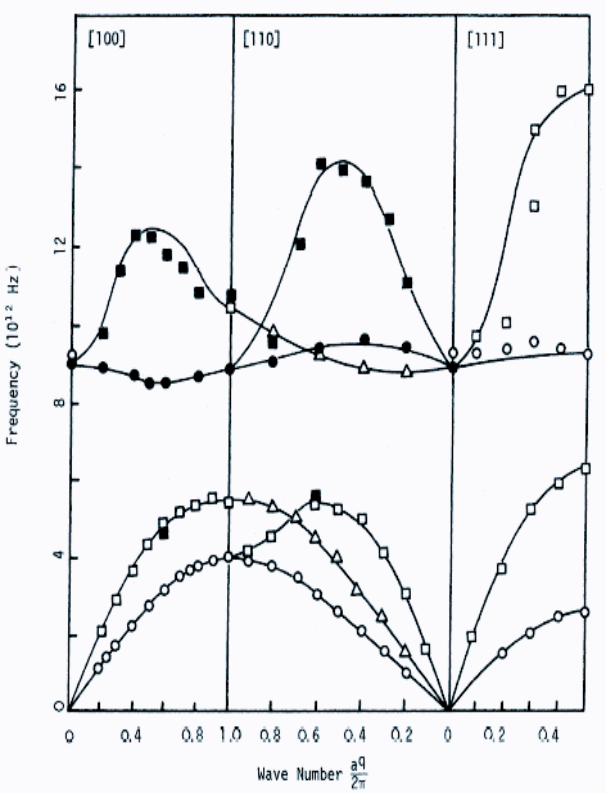

Figure 5.27: Phonon dispersion curves in $PdD_{0.63}$, □,■, ∘, •, show experimental points and (—) represent model calculation [Rafizadeh 1981].

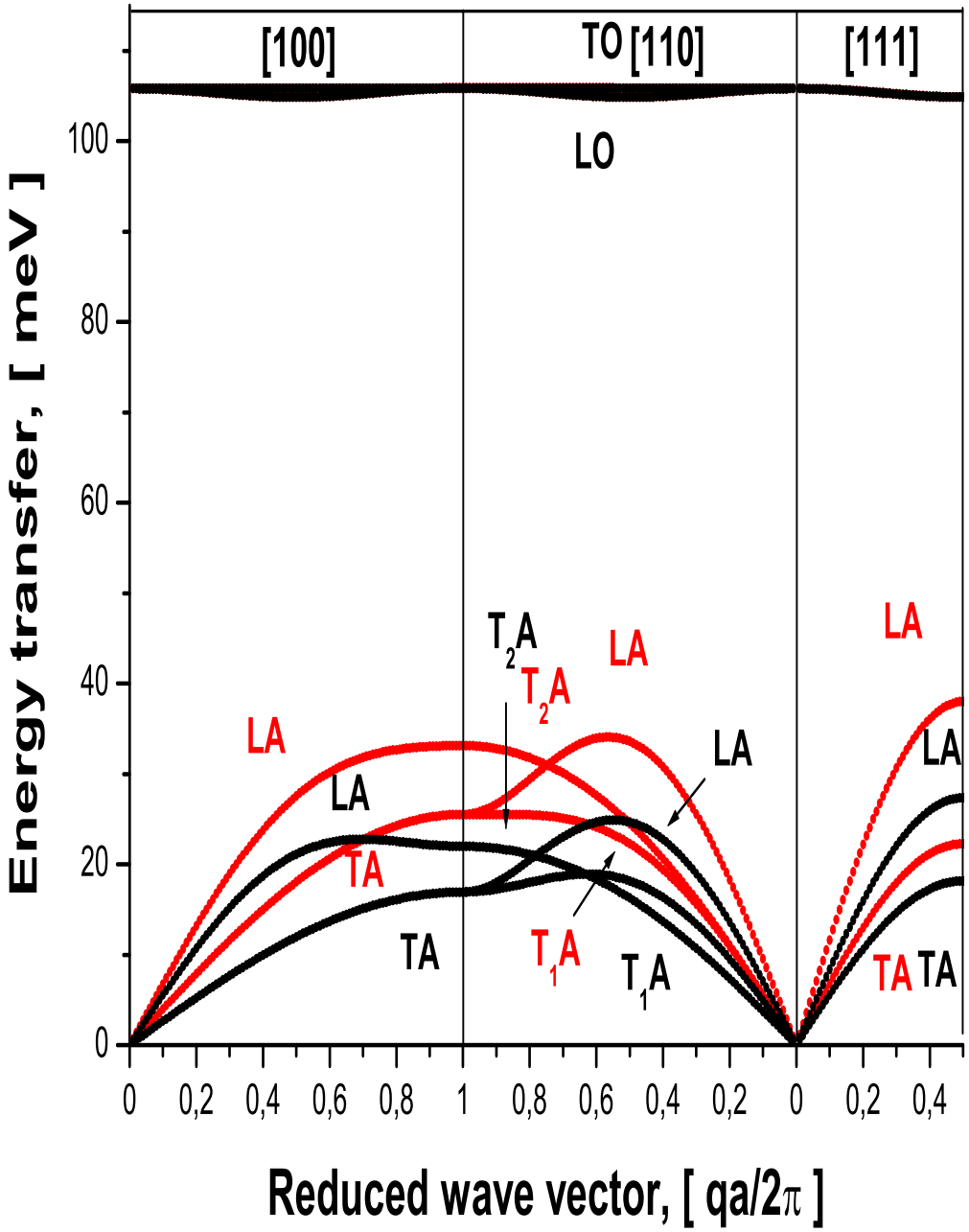

Figure 5.28: Calculated phonon dispersion curves in fully hydrogenated austenitic stainless steels,(—) with and (—) without correction due to Grüneisen parameter.

From the result of the calculation on phonon dispersion curves the influence of Grüneisen parameter is clearly seen. Influence of changes of metal-metal force constants on optic modes are extremely small. In the acoustic region phonon dispersion branches are not just rescaled, they also had change of the shape (fig. 5.28). In (fig. 5.29) only acoustic branches were presented. It was compared with acoustics in system without hydrogen and also with calculation of phonon dispersion curves with hydrogen but without correction due to the Grünseisen parameter. Graphs which take the Grünseisen parameter into account were rescaled for easier comparison. In the direction (100) transversal mode stay unchanged but longitudinal is significantly changed in the way that shape of phonon dispersion curve gain maximum at a value of reduced wave vector of 0.7. In the direction (110) T_2 stay unchanged. The longitudinal branch gain local maximum similar to T_1. Value of local minimum in T_1 is greatly increased. In the direction (111) the shape of phonon dispersion curves stay untouched but they are shifted to higher values. This is much more pronounced in transversal direction. All this behaviour is observed in both hydrogenated systems. This behaviour of phonon dispersion curves is more pronounced when correction due to lattice expansion is included, because in this case bonding between metal atoms is much weaker. Comparison of phonon dispersion curves in hydrogenated austenitic stainless steels with UC system(fig. 5.26, 5.28) shows great similarity of phonon dispersion curves and it is opposite to Pd-D system(fig. 5.27) in acoustic modes, even branches T_1 and T_2 intersect on similar point with q=0.7. Optic modes shows higher dispersion which correspond to smaller mass ratio.

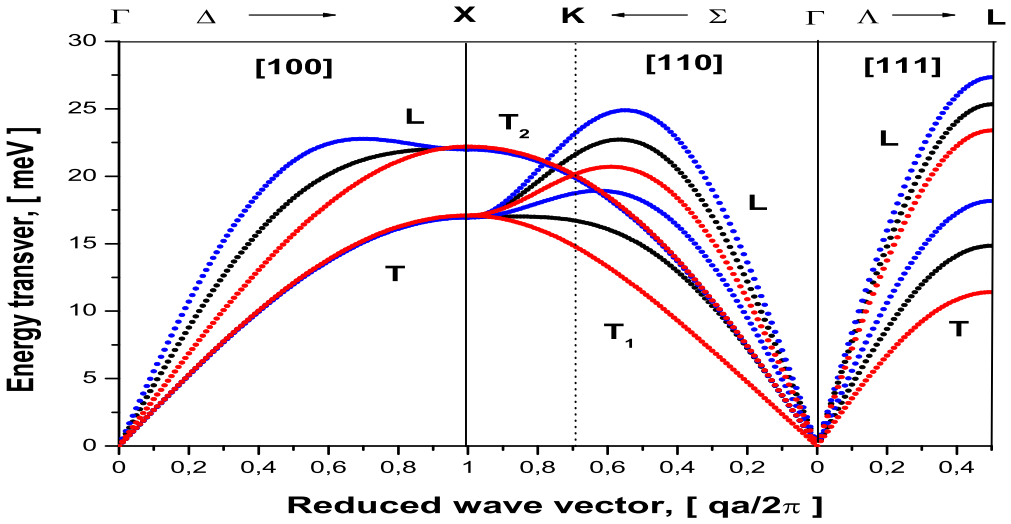

Figure 5.29: Calculated phonon dispersion curves in (○)austenitic stainless steel without hydrogen, with hydrogen(○) and after correction due to Grüneisen parameter(○) without correction due to Grüneisen parameter but rescaled for comparison.

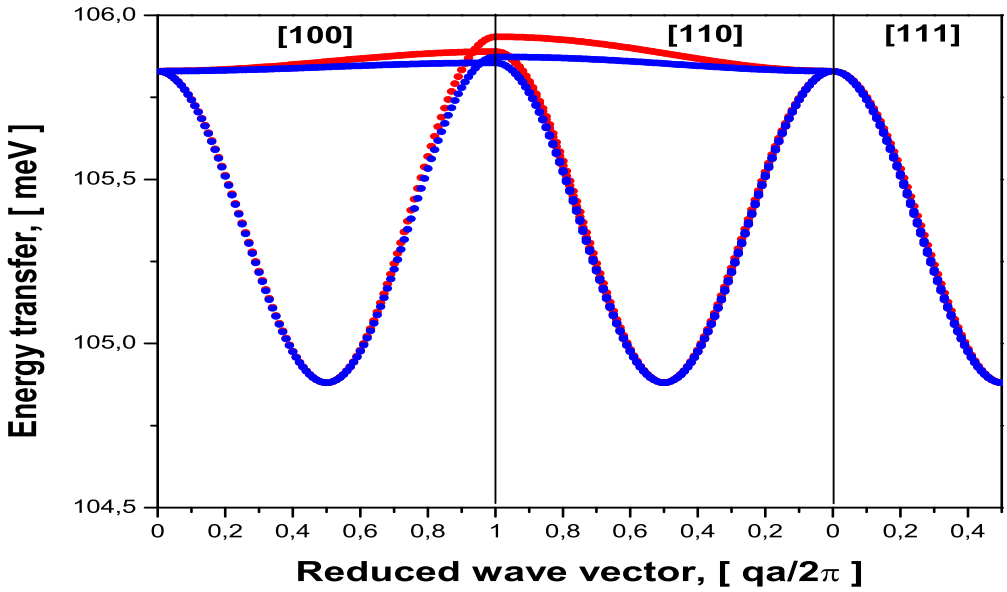

Figure 5.30: Calculated phonon dispersion curves with hydrogen(○) and after correction due to Grüneisen parameter(○) without correction due to Grüneisen parameter.

Optic modes are very narrow with width of 1-1.5 meV(fig. 5.30) which correspond to relation (eq. 5.6). Influence of correction of metal-metal force on the optic modes due to Grüneisen parameter are extremely small (less than 0.1 meV). Greatest difference are in longitudinal mode in [100] direction and in transversal in [110] direction, all other modes are almost identical.
From the model calculation the phonon density of states was obtained. It was also included the influence of the resolution function which was obtained from the curve of FWHM as function of neutron energy loss for the FANS spectrometer. In the acoustic region FWHM is between 1 and 3 meV respectively with quadratic dependence between them. In the optic region FWHM is close to 5 meV.

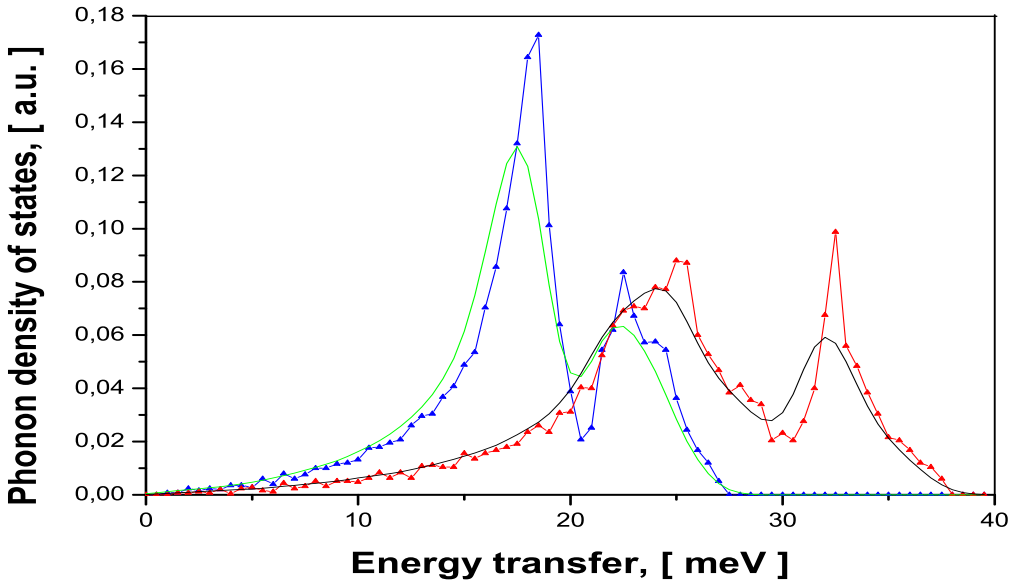

Figure 5.31: Calculated acoustic part of phonon density of states in fully hydrogenated austenitic stainless steel without correction of Grüneisen parameter(-▲-) and simulated resolution function(—) and after correction due to Grüneisen parameter(-▲-) and simulated resolution function(—).

Discrepancy between model and experiment could be explained by influence of H-H bonding and different alloying elements.

Hydrogen-hydrogen interaction

Dispersion could be also caused by lattice dynamics, two main source of contribution are hydrogen-hydrogen interaction and influence of different alloying elements. Firstly simulation will be performed with separate effects and finally both contributions will be taken into account. To reduce the discrepancy between simulation and experiment hydrogen-hydrogen interaction was introduced. It was parameterised with 3 independent parameters. Simulation was performed in the way that difference between experimental data (DOS) for fully hydrogenated system and simulation which include Born-von Karman model with correction due to resolution function was minimal. Standard non-linear fit procedure is not possible due to lots of numerical error (background, non-complete spectra, numerical errors). The obtained set of parameter for H-H interaction as well as for Me-H is not unique. From these parameters phonon dispersion curves were calculated. As input parameters for metal-metal interaction were used data from single crystal phonon dispersion curves. These values were corrected for Grüneisen parameter.

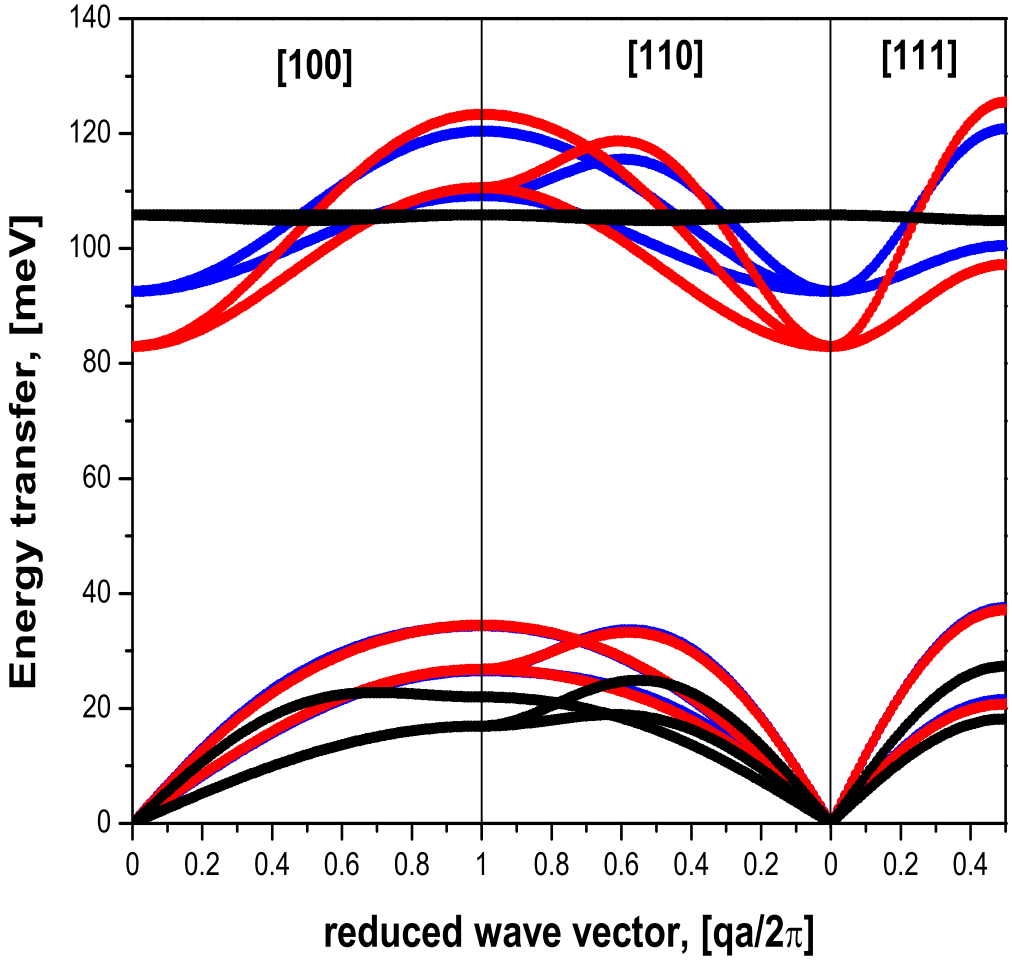

Figure 5.32: Phonon dispersion curves for fully hydrogenated austenitic stainless steels, (Fe-18Cr-10Ni) (—) Born-von Karman model with H-H interaction, (Fe-25Cr-20Ni) (—) Born-von Karman model with H-H interaction and (—) without it.

From the calculated phonon dispersion curves it is easy to see that influence of the hydrogen-hydrogen bonding on the acoustic modes is very small. Only clear difference could be seen in longitudinal mode in [100] direction and in transversal in [110] direction, all other modes are almost identical. On the other hand it is easy to see that hydrogen-hydrogen interactions strongly increase dispersion in optics modes. From the obtained set of parameter for force constants phonon density of states were calculated. In comparison with UC (fig. 5.26) and Pd-D system (fig. 5.26) it is straightforward that the acoustic

modes in hydrogenated austenitic stainless steels is almost identical to Pd-D system. In the optic modes also considerable similarity exist especially in direction [111]. Also calculated density of states are very similar.

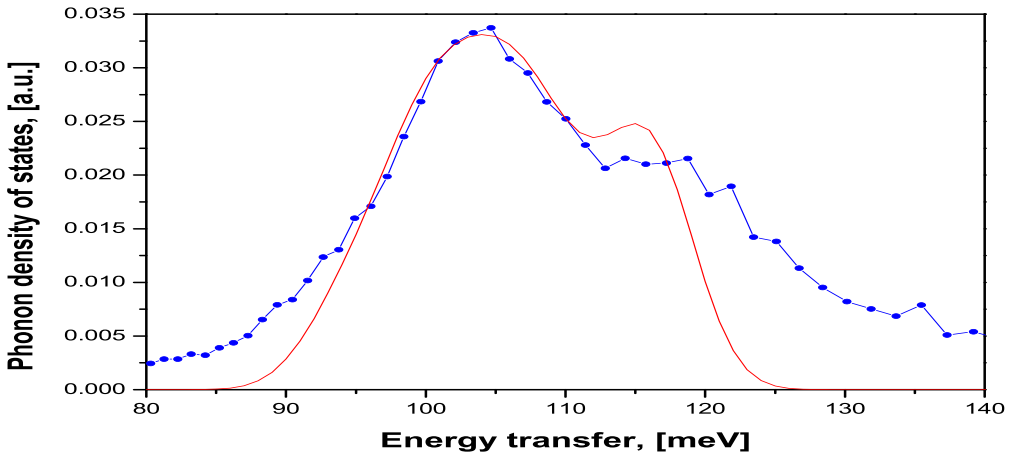

Figure 5.33: Phonon density of states for hydrogen modes in fully hydrogenated austenitic stainless steel(Fe-18Cr-10Ni), (-●-) experimental data, (—) calculation based on the Born-von Karman model convoluted with resolution function.

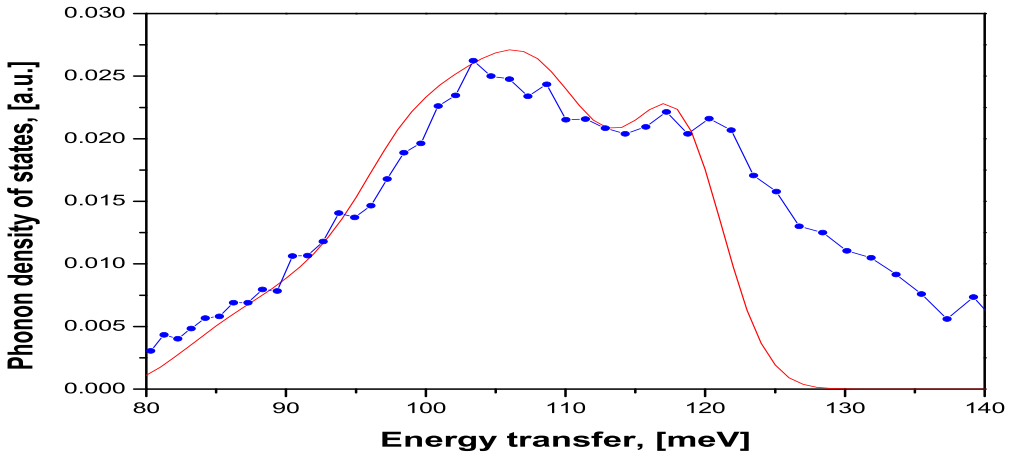

Figure 5.34: Phonon density of states for hydrogen modes in fully hydrogenated austenitic stainless steel(Fe-25Cr-20Ni), (-●-) experimental data, (—) calculation based on Born-von Karman model convoluted with resolution function.

From the simulation the introduction of hydrogen-hydrogen bonding could explain a broadning of the hydrogen peak pretty well but could not simulate ratio of intensity between transversal and longitudinal peak as well as distance between them. In the further step of the calculation the influence of alloying elements on the phonon density of states was simulated. The mean problem in this simulation is that influence of hydrogen-hydrogen bonding is overestimated. In further calculation different influence of alloying elements were taken into account with neglected hydrogen-hydrogen interaction.

Alloying effects

Due to different alloying elements hydrogen atoms are in changed interatomic potential which first change energies of metal-hydrogen bondings and also break isotropy. As a consequence anharmonicity appears. When different alloying elements are not taken into account all atoms are treated as mean atoms with average energy of metal-hydrogen interaction. Different alloying elements are taken into account only through the shifting of energy for given configuration but hydrogen atoms stay in the centre of octahedra. As input for the modelling in the frame of Born-von Karman model energies of different configurations of hydrogen neighbourhood are used. For every different surroundings of hydrogen atom dynamical matrix and corresponding phonon density of states were calculated. All configuration which more probable than 1% are taken into account with corresponding weights.

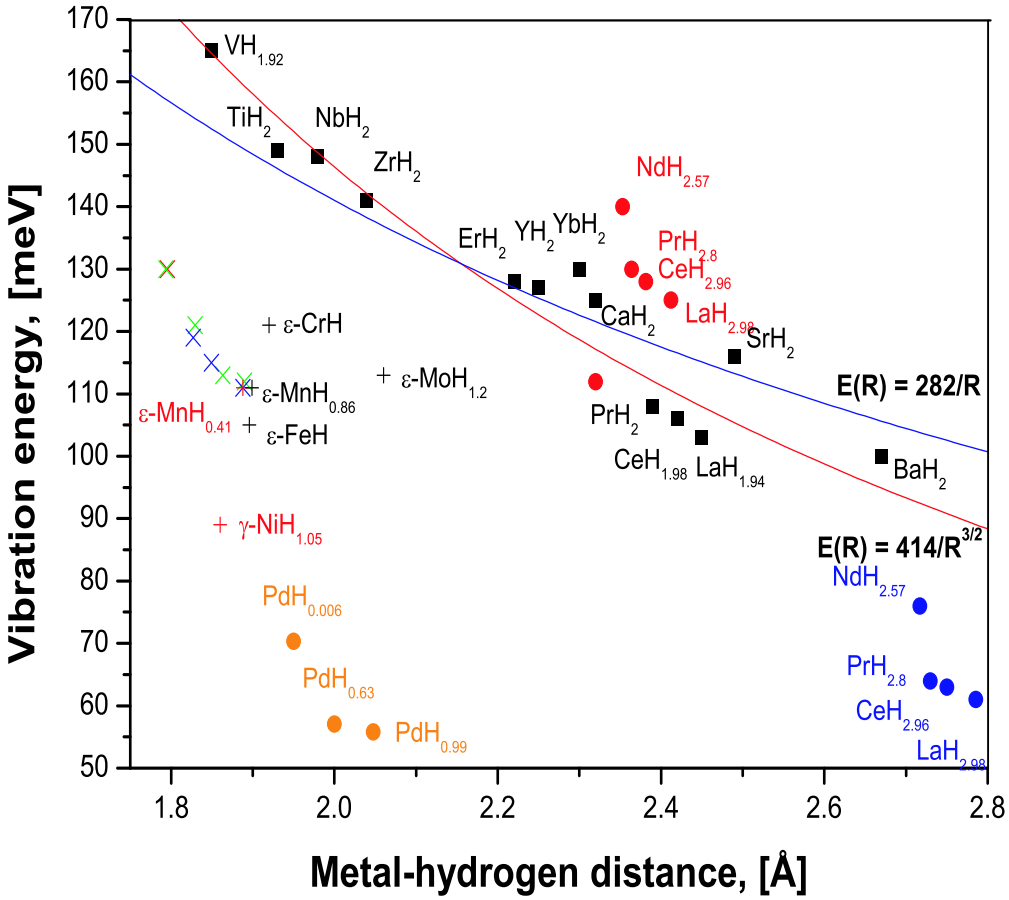

Figure 5.35: Vibration energy of hydrogen in different metal-hydrogen systems:
■ MeH_2 with CaF_2 structure
● MeH_{2-3} hcp with H in tetrahedral voids
● MeH_{2-3} hcp with H in octahedral voids
● Pd-H systems
+ MeH_x with NaCl structure
+ MeH_x with NiAs structure
× hydrogenated Fe-25Cr-20Ni
× hydrogenated Fe-18Cr-10Ni
× hydrogenated Fe-18Cr-16Ni-10Mn.
All presented systems crystalise in face centred cubic or hexagonal close packing.

Table 5.4: Vibration energy in metal hydrides of transition metals. ε' was obtained for metal-hydrogen distance R=1.885 Å.

System	Space group	ε[meV]	R[Å]	ε'[meV]	reference
γ - $NiH_{1.05}$	$Fm\bar{3}m$	89	1.86	87	[Dorner 1989]
ε' - FeH	$P6_3/mmc$	105	1.8958	105	[Cornell 1997]
γ - $MnH_{0.41}$	$Fm\bar{3}m$	111	1.8888	111	[Antonov 2000]
ε - $MnH_{0.86}$	$P6_3/mmc$	111	1.899	112	[Kolesnikov 1991]
ε - CrH	$P6_3/mmc$	121	1.92	124	[Cornell 1997]

Corrections on the distance was made in the way that $\varepsilon \sim R^{-3/2}$. For the calculation of energy ε' as metal-metal distance the value is used for fully hydrogenated system. ε' correspond to the actual metal-hydrogen distance. The energy of the metal-hydrogen interaction was calculated as a linear combination of corrected energies of the neighbouring metal-hydrogen interactions. This approximation assume that all metal-hydrogen distances are the same with hydrogen atoms located in the middle of octahedra.
In this model, all possible neighbourhood configurations were taken into account and in calculation of DOS only these configurations were applied which are more probable than 1%. This simulation is based on a random alloy assumption. Calculation was performed in the way that for all distributions which are taken into account, dynamical matrices were calculated. From the dynamical matrices densities of states were obtained. All DOS were multiplied with the probability that specific configuration of metal atoms occur.

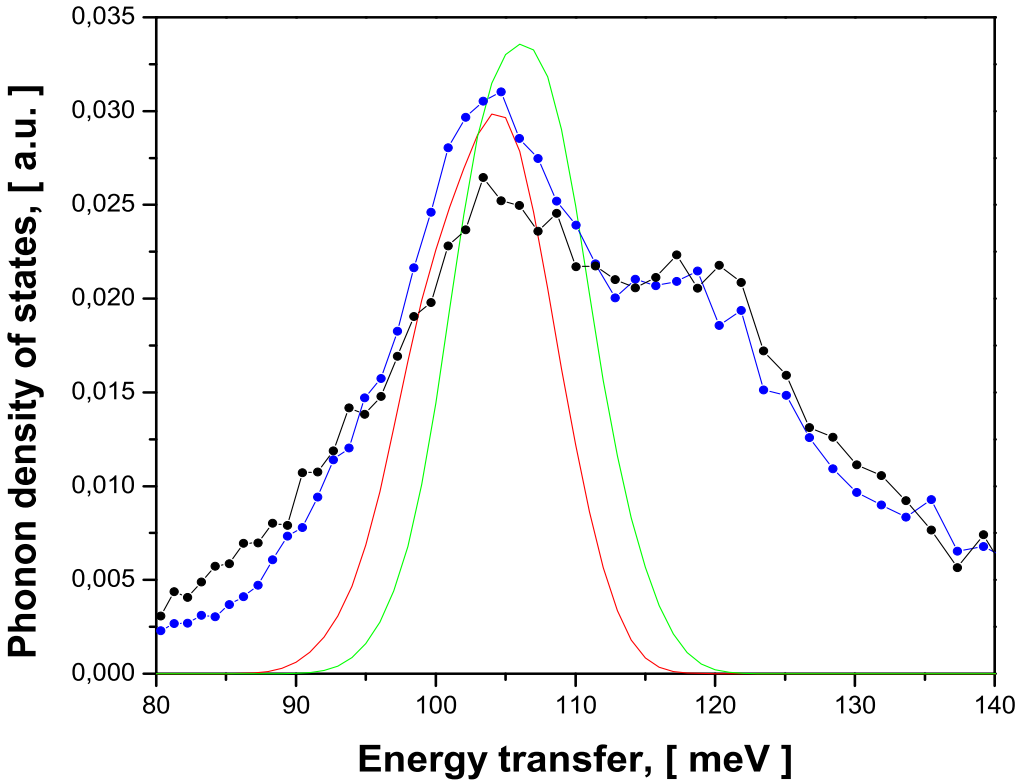

Figure 5.36: Influence of different alloying elements on phonon density of states for hydrogen modes in fully hydrogenated austenitic stainless steel(Fe-18Cr-10Ni), (-●-) experimental data, (—) calculation based on Born-von Karman model convoluted with resolution function. Phonon DOS in fully hydrogenated austenitic stainless steel(Fe-25Cr-20Ni), (-●-) experimental data, (—) calculation based on Born-von Karman model convoluted with resolution function.

Hydrogen-hydrogen interaction and alloying effects

From the comparison of these two simulations the influence of alloying elements and hydrogen-hydrogen interaction, it is easy to see that contribution of hydrogen-hydrogen interaction is the dominant term in description of the phonon density of states. This is especially pronounced for Fe-18Cr-10Ni. When only the contribution of H-H interaction is applied, the interaction term is overestimated due to fitting procedure. In the next step both terms will be taken into account. The parameters obtained for interatomic interaction will be used for simulation of DOS in samples with medium and low hydrogen content.

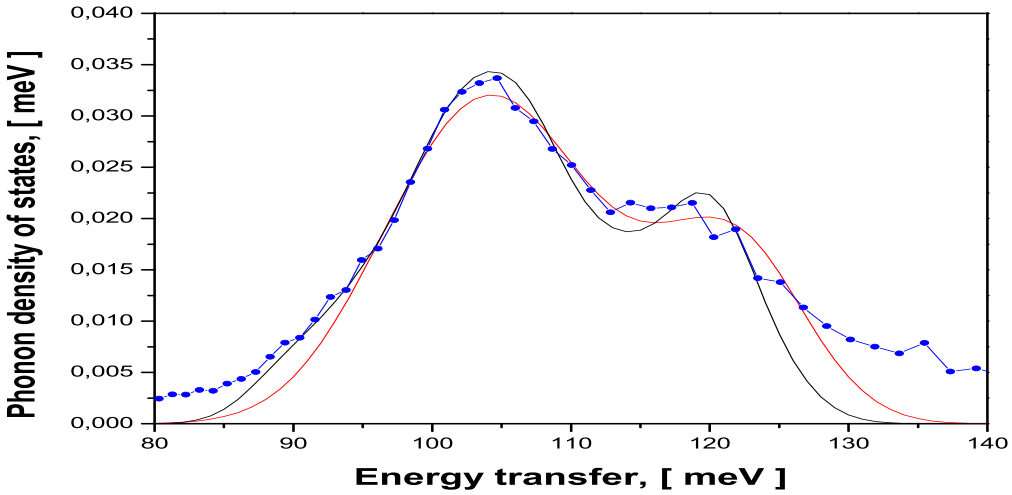

Figure 5.37: Influence of different alloying elements on phonon density of states for hydrogen modes in fully hydrogenated austenitic stainless steel Fe-18Ni-10Cr, (-●-) experimental data, (—) calculation based on Born-von Karman model with hydrogen-hydrogen interaction and with different alloying elements and (—) only with hydrogen-hydrogen interaction.

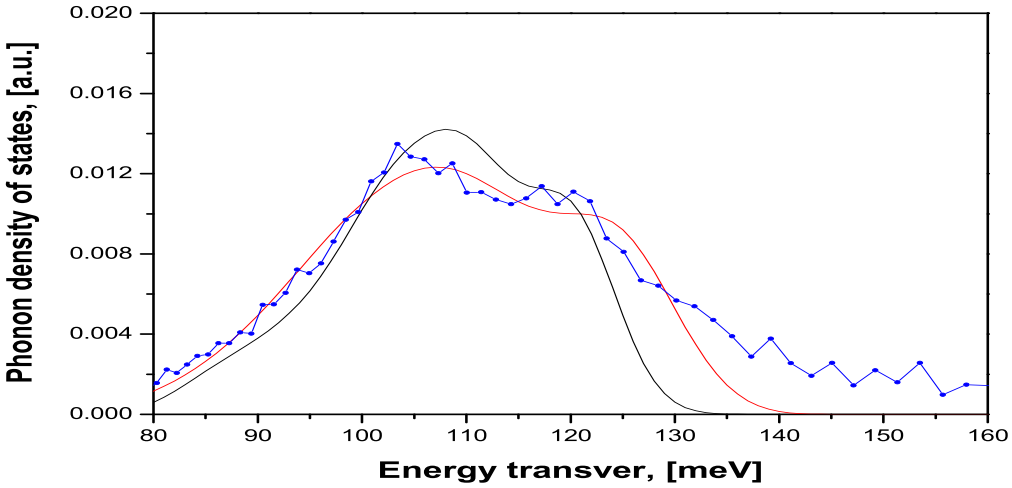

Figure 5.38: Influence of different alloying elements on the phonon density of states for hydrogen modes in fully hydrogenated austenitic stainless steel Fe-25Ni-20Cr, (-●-) experimental data, (—) calculation based on Born-von Karman model with hydrogen-hydrogen interaction and with different alloying elements and (—) only with hydrogen-hydrogen interaction.

After applying of both terms, a better fitting was obtained. In the same time adding a contribution of alloying elements in the model will reduce the strength of hydrogen-hydrogen interaction of about 50%. The obtained values for hydrogen-hydrogen force constants in austenitic stainless steel Fe-18Ni-10Cr are thus much more realistic than before.

Table 5.5: Comparison of hydrogen-hydrogen force constants in Born-von Karman model with hydrogen-hydrogen force constants reported by [Rafizadeh 1981]. In [Rafizadeh 1981] the fitting parameters for D-D interaction are derived from second neighbour Born-von Karman model.

force constant	Fe-18Ni-10Cr	Fe-25Ni-20Cr	$PdD_{0.63}$[Rafizadeh 1981]
α_{11} [N/m]	4.0[this study]	3.0[this study]	3.7[Rafizadeh 1981]
β_{11} [N/m]	0.7[this study]	-0.6[this study]	-0.45[Rafizadeh 1981]
α_{12} [N/m]	4.0[this study]	3.0[this study]	2.96[Rafizadeh 1981]
α_{21} [N/m]	-	-	-0.17[Rafizadeh 1981]
α_{22} [N/m]	-	-	3.33[Rafizadeh 1981]

Increased quality of simulation is especially pronounced in the region about 110-125 meV, which is connected to the longitudinal peak.
In the case of the austenitic stainless steel Fe-25Ni-20Cr the influence of different alloying elements is even more pronounced. This simulation fit experimental data well in all regions except the high energy part (over 135 meV). Simulation is slightly better than in Fe-18Ni-10Cr, the main difference is in the low energy part. Part of discrepancy could be explained due to phase transition. In the high energy region(over 135 meV) the discrepancy between experiment and theory is mainly due to multiphonon processes and background substraction.

5.3.2 Modelling of medium hydrogenated samples

For modelling of non-stoichiometric metal hydrides MeH_x($0.1<x<0.9$) in the frame of Born-von Karman model two different approaches could be applied: building of a large supercell or using averaging methods [Rafizadeh 1981]. This model was based on the following assumptions: that mass of hydrogen was substituted with average mass of hydrogen in octahedral sites and force constants are substituted with average force constants metal-hydrogen and hydrogen-hydrogen respectively (see table 5.6).

Table 5.6: Comparison of Born-von Karman model with average method proposed by [Rafizadeh 1981] where x is hydrogen metal ratio.

Physical quantity	Born-von Karman model	averaging method [Rafizadeh 1981]
mass of hydrogen	m_H	xm_H
force constants Me-H	ϕ_{Me-H}	$x\phi_{Me-H}$
force constants H-H	ϕ_{H-H}	$x^2\phi_{H-H}$

These values were introduced in the dynamical matrix which was diagonalised. [Rafizadeh 1981] has applied this model on the $PdD_{0.63}$ system. First simulated phonon dispersion curves and density of states were presented. From these graphs is easy to estimate the influence of hydrogen content.

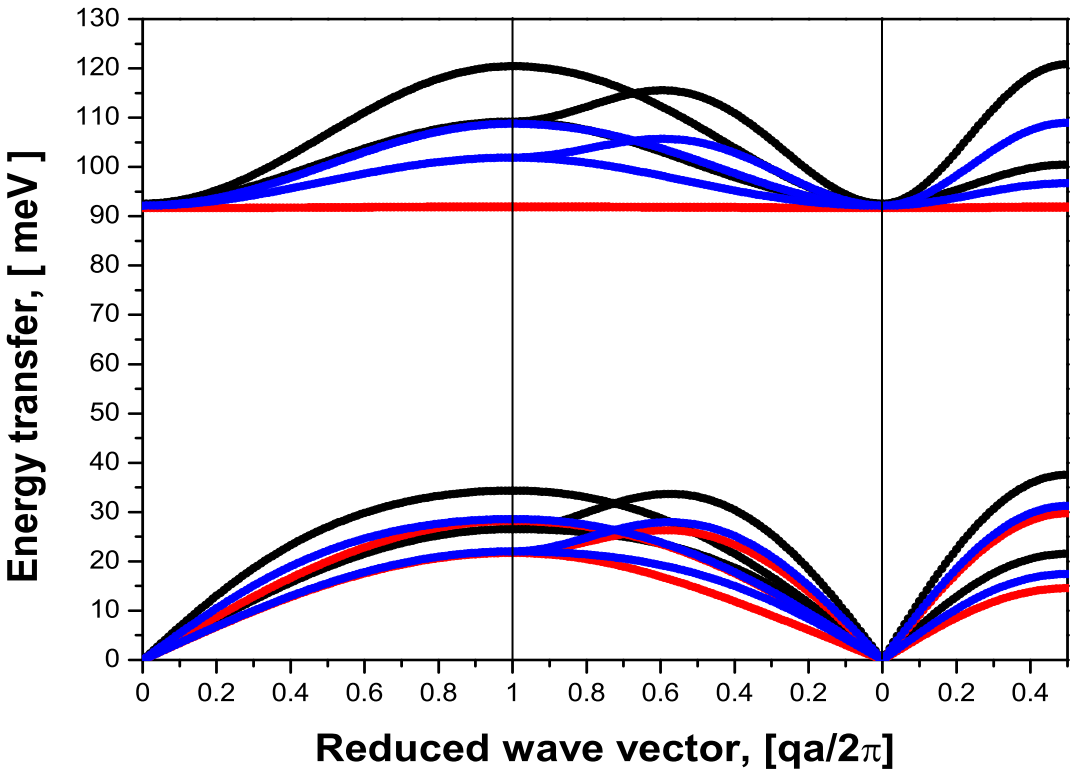

Figure 5.39: Simulation of influence of different concentration of hydrogen on the phonon dispersion curves, (-●-) for H/Me=1, (-●-) H/Me=0.56 and (-●-) H/Me=0.01 with the same interatomic force constants.

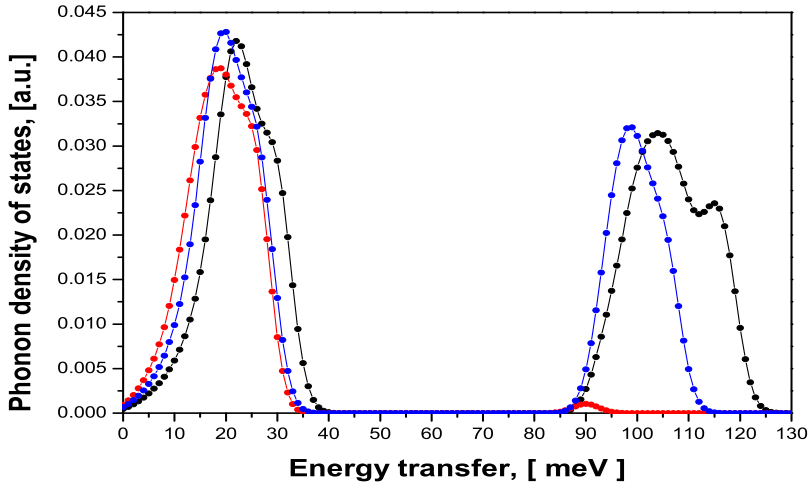

Figure 5.40: Simulation of influence of different concentration of hydrogen on the phonon density of states, (-●-) for H/Me=1, (-●-) H/Me=0.56 and (-●-) H/Me=0.01 with the same interatomic force constants. Contribution of resolution function is included.

From the graph of the phonon dispersion curves it is visible that the concentration of hydrogen with same force constants has great impact on lattice dynamics. In the acoustic region significant softening (15-20%) was obtained when the concentration(x) of hydrogen was reduced from 100 to 50%, below 50% the influence of hydrogen on the acoustic modes is very low. The shape of phonon dispersion curves does not vary due to different hydrogen content. In the optical part of phonon dispersion curve influence of different values of x is much more pronounced. Broadness of optical modes is almost a linear function of concentration, so in the limit of low hydrogen content this model corresponds to the system of Einstein oscillators. Values for interatomic forces were obtained from simulation on fully hydrogenated austenitic stainless steels Fe-25Cr-20Ni and Fe-18Cr-10Ni. Force constants are function of lattice parameters. In first approximation the H-H interactions are assumed to be independent of lattice expansion due to hydrogenation. Force constants between metal atoms were corrected due to Grüneisen parameter and the metal-hydrogen interaction was corrected with the empirical relation that E is proportional to $\mathrm{R}^{-3/2}$. Lattice parameters for different occupancy were obtained from diffraction studies.

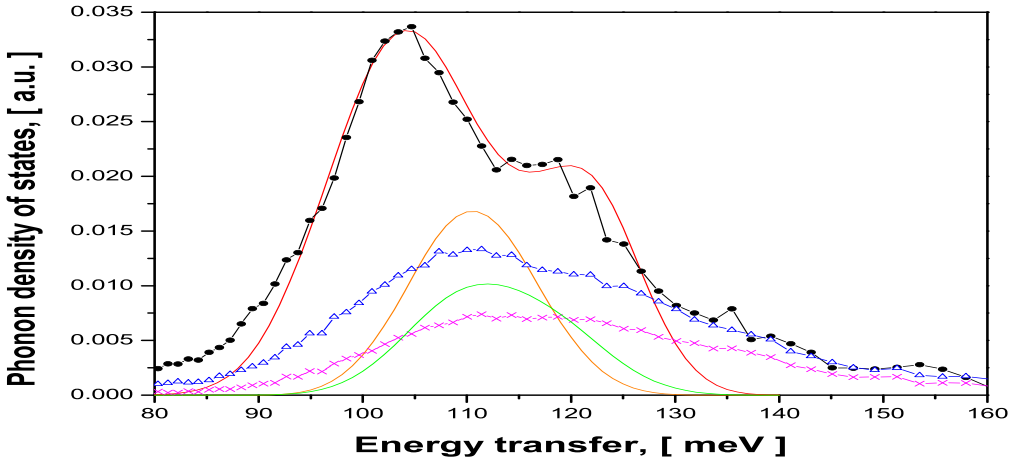

Figure 5.41: Simulation of phonon density of states for different hydrogen loading in hydrogenated austenitic stainless steel Fe-18Ni-10Cr, experimental data for H/Me=0.94(5)(-●-) , (-△-) H/Me=0.56(5), H/Me=0.30(4) (-×-) and model calculation H/Me=0.94(5)(—), (—) H/Me=0.56(5), H/Me=0.30(3) (—) respectively. This model just only use obtained force constants for fully hydrogenated system.

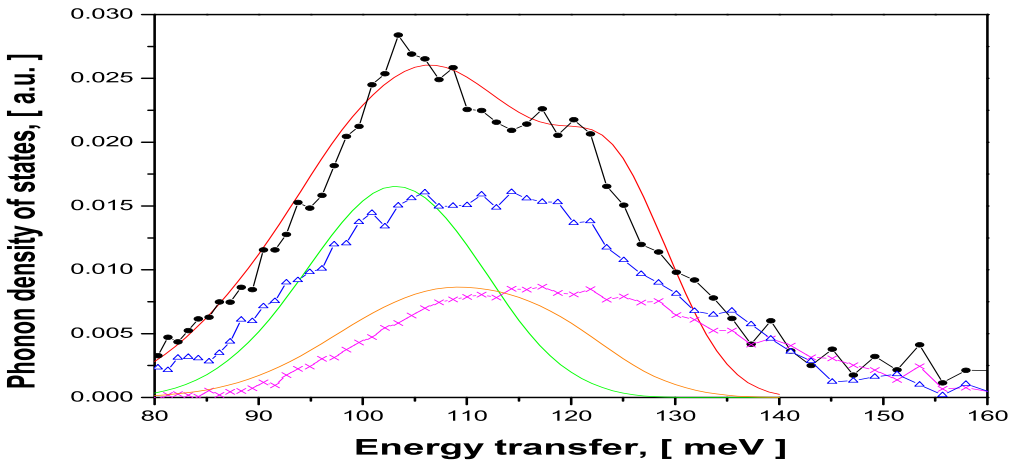

Figure 5.42: Simulation of phonon density of states for different hydrogen loading in hydrogenated austenitic stainless steel Fe-25Ni-20Cr, experimental data for H/Me=1.03(9)(-●-) , (-△-) H/Me=0.66(3), H/Me=0.35(2)(-×-) and model calculation H/Me=1.03(9)(—), (—) H/Me=0.66(5), H/Me=0.35(2) (-×-) respectively. This model use only obtained force constants for fully hydrogenated system.